Swimming Dynamics of the Lyme Disease Spirochete

Dhruv K. Vig[1,3] and Charles W. Wolgemuth[1,2,3,4]

[1]Center for Cell Analysis and Modeling, University of Connecticut Health Center, Farmington, Connecticut 06030-6406, USA
[2]Department of Cell Biology, University of Connecticut Health Center, Farmington, Connecticut 06030-6406, USA
[3]Department of Molecular and Cellular Biology, University of Arizona, Tucson, Arizona 85721, USA
[4]Department of Physics, University of Arizona, Tucson, Arizona 85721, USA

(Received 28 June 2012; revised manuscript received 10 September 2012; published 21 November 2012)

The Lyme disease spirochete, *Borrelia burgdorferi*, swims by undulating its cell body in the form of a traveling flat wave, a process driven by rotating internal flagella. We study *B. burgdorferi*'s swimming by treating the cell body and flagella as linearly elastic filaments. The dynamics of the cell are then determined from the balance between elastic and resistive forces and moments. We find that planar, traveling waves only exist when the flagella are effectively anchored at both ends of the bacterium and that these traveling flat waves rotate as they undulate. The model predicts how the undulation frequency is related to the torque from the flagellar motors and how the stiffness of the cell body and flagella affect the undulations and morphology.

DOI: 10.1103/PhysRevLett.109.218104 PACS numbers: 47.63.Gd, 87.85.gf, 87.85.gj

The spirochetes are a unique group of motile bacteria that are notable for their long, thin, planar wave-like or helical morphologies [1]. In order to move, the spirochetes undulate or rotate their cell body, as opposed to rotating external organelles, such as the ubiquitous helical bacterial flagellum. The spirochetes do still use flagella to move; however, spirochetal flagella are encased in the periplasm of the cell, which is the narrow space (~ 30 nm) between the inner and outer membranes [2]. Rotation of the flagella in this space causes the rotations and undulations of the cell body that drive the movement of these cells through their environments.

Here we focus on *Borrelia burgdorferi*, the causative agent of Lyme disease, the most prevalent vector-borne illness in the United States [3]. During its enzootic cycle, *B. burgdorferi* swims through a myriad of viscous fluids and polymeric environments, such as blood and the extracellular matrix [4,5]. Unlike other bacteria whose motility would be inhibited in these environments, these spirochetes maneuver through them by undulating the entire ~ 10 μm length of their ~ 0.3 μm diameter bodies as a planar, traveling wave [6,7]. In *B. burgdorferi*, there are 7 to 11 flagella attached to flagellar motors near each end of the bacterium; the flagella wrap inward down the length of the cell body and are long enough to overlap at the cell middle with flagella emanating from the other end [8,9]. Because the flagella are encased in the periplasm, rotation of the flagella causes the cell body to undulate, which, in turn, produces the force that propels the cell [6,9] [Fig. 1(a)].

The preceding explanation, though, is deceptive; the physics by which rotation of helical flagella in the periplasmic space produces the roughly planar traveling waves of the cell body remains unclear. In order for the flagella to reside in the periplasmic space, they must bend. The elastic forces required to bend the flagella cause the cell body to bend into the characteristic flat-wave shape of *B. burgdorferi*, via Newton's third law [10]. When the flagella are rotated, they must continually deform, and the force and

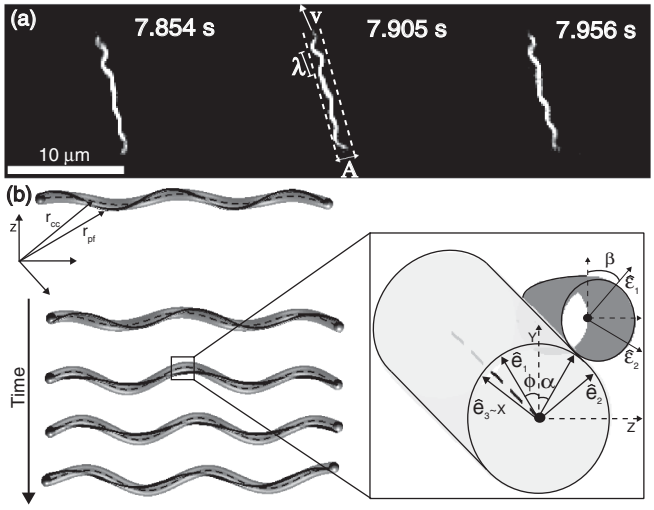

FIG. 1. (a) Time course of the swimming of *B. burgdorferi* [21]. Over the 0.1 s shown here, the cell undulates slightly more than half a period; i.e., the frequency is $\omega \sim 10\pi$ s^{-1}. The cell has wavelength $\lambda \sim 3.0$ μm and amplitude $\mathcal{A} \sim 1.0$ μm. Over this 0.1 s, the cell moves slightly up the page, with a swimming speed that is proportional to $\mathcal{A}^2\omega/\lambda$ [6,19,20]. (b) The periplasmic flagella (dark gray) are constrained to lie on the surface of the cell body (light gray). Rotation of the flagella produces rotation and undulation of the cell body. We use orthonormal triads at each point along the centerlines of the flagella and cell body to define the local orientations of these filamentary objects. For example, the periplasmic flagella are located in the direction $-\sin\alpha\hat{\mathbf{y}} + \cos\alpha\hat{\mathbf{z}}$ from the centerline of the cell body, where α is the angle of rotation with respect to $\hat{\mathbf{y}}$. See text for further details.

torque balance between the flagella and the cell must conspire to produce traveling waves along the cell body. In this Letter, we examine the physics by which flagellar rotation produces these periodic undulations of the cell body. Our work is similar to previous work on *Leptospira* [11]; however, we take into account the finite size of the cell radius and a more complete description of the resistive forces between the cell body and flagella. While we focus on the swimming dynamics of *B. burgdorferi*, it is likely that our results are generally applicable to the physics of spirochete locomotion, and specifically to *Treponema pallidum*, the spirochete that causes syphilis, which also has a flat-wave morphology [12].

In order to construct a dynamic model for the swimming motility of *B. burgdorferi*, we treat the cell body and periplasmic flagella as elastic filaments. The flagella in *B. burgdorferi* form a ribbon-like structure that is localized circumferentially in the periplasm [2]. Therefore, we further assume that the flagella can be treated as a single elastic filament, as has been done previously to describe the static conformation of *B. burgdorferi* [10]. The shape of the cell body and flagella are then defined by the positions of their centerlines, $\mathbf{r}_c$ and $\mathbf{r}_f$, respectively, and we define a local, orthonormal triad for the cell body $[\hat{\mathbf{e}}_1,\hat{\mathbf{e}}_2,\hat{\mathbf{e}}_3]$, where $\hat{\mathbf{e}}_3$ is the tangent vector, and $\hat{\mathbf{e}}_1$ points to material points on the surface of the cell body, and a similar orthonormal triad $[\hat{\boldsymbol{\varepsilon}}_1, \hat{\boldsymbol{\varepsilon}}_2, \hat{\boldsymbol{\varepsilon}}_3]$ for the flagella [Fig. 1(b)]. The strain vectors for the cell body and flagella, $\boldsymbol{\Omega}$ and $\boldsymbol{\varpi}$, respectively, are related to the spatial derivatives of the orthonormal triads as $\frac{\partial \hat{\mathbf{e}}_i}{\partial s} = \boldsymbol{\Omega} \times \hat{\mathbf{e}}_i$ and $\frac{\partial \hat{\boldsymbol{\varepsilon}}_i}{\partial s} = \boldsymbol{\varpi} \times \hat{\boldsymbol{\varepsilon}}_i$, where $i = 1, 2, 3$. Because the flagella reside in the periplasmic space, their position can be written in terms of the centerline of the cell body, $\mathbf{r}_f = \mathbf{r}_c + a\hat{\mathbf{p}}_1$, where a is the radius of the cell body and $\hat{\mathbf{p}}_1$ points from the centerline of the cell body to the flagella [Fig. 1(b)].

The amplitude of the shape of *B. burgdorferi* is smaller than the wavelength. We, therefore, consider the small amplitude dynamics of a cell aligned predominantly with the x axis, $\mathbf{r}_c = x\hat{\mathbf{x}} + y(x)\hat{\mathbf{y}} + z(x)\hat{\mathbf{z}}$. (This approximation is not entirely justified as the ratio $2\pi\mathcal{A}/\lambda \sim 1$. Therefore, the results of our model may not quantitatively match observations of *B. burgdorferi*, but we expect they will still capture the dynamics qualitatively.) The location of the flagella can then be defined by the angle with respect to the y axis, $\alpha(x)$ [Fig. 1(b)]. We also define the angles ϕ and β which describe the rotation of the orthonormal triads about the tangent vectors of the cell body and flagella, respectively [Fig. 1(b)]. The twist densities are then $\Omega_3 \approx \partial\beta/\partial x$ and $\varpi_3 \approx \partial\phi/\partial x$.

In mutants lacking flagella, the equilibrium shape of *B. burgdorferi* is straight; purified flagella are preferentially helical with preferred curvature $\kappa_0 \sim 1.5\ \mu\text{m}^{-1}$ and torsion $\tau_0 \sim 1.2\ \mu\text{m}^{-1}$ [10]. Treating the cell body and flagella as linearly elastic filaments, the restoring moments for these filaments are related to the strain vectors as

$$\mathbf{M}_c = A_c\Omega_1\hat{\mathbf{e}}_1 + A_c\Omega_2\hat{\mathbf{e}}_2 + C_c\Omega_3\hat{\mathbf{e}}_3, \quad (1)$$

$$\mathbf{M}_f = A_f(\varpi_1 - \kappa_0)\hat{\boldsymbol{\varepsilon}}_1 + A_f\varpi_2\hat{\boldsymbol{\varepsilon}}_2 + C_f(\varpi_3 - \tau_0)\hat{\boldsymbol{\varepsilon}}_3, \quad (2)$$

where A_c and A_f are the bending moduli and C_c and C_f are the twist moduli for the cell body and periplasmic flagella, respectively. For simplicity, we assume that $C_f = A_f$ and $C_c = A_c$ [13].

The dynamics of the cell body and flagella are defined through force and moment balance equations that equate the elastic restoring forces to the resistive forces. Movement of the cell body through the external fluid is resisted by fluid drag, which is modeled here using resistive force theory [14]. In the small amplitude approximation, we need only consider movements perpendicular to the tangent vector of the cell body which are resisted by a force proportional to the velocity with drag coefficient $\zeta_\perp \sim 4\pi\eta$, where η is the viscosity of the fluid. Rotation of the cell body about its tangent vector experiences a resistive torque proportional to $\partial\phi/\partial t$, with rotational drag coefficient ζ_r. In addition to these forces and torques from the external fluid, movement of the flagella within the periplasmic space also produces resistive forces and torques. Recently, Yang *et al.* showed that rotation of the periplasmic flagella with respect to the cell body at speed produces a resistive force proportional to the speed $\omega_u = d\beta/dt - d\alpha/dt$, and the resistive force is likely negligible [15]. Similarly, they showed that translation of the flagella in the periplasm produced a resistive force, with negligible torque. We define the drag coefficients for rotation and translation of the flagella to be ζ_β and ζ_α. The force and moment balance equations are then [13]

$$\frac{d\mathbf{F}_c}{dx} + \mathbf{K} = \zeta_\perp\left(\frac{dy}{dt}\hat{\mathbf{y}} + \frac{dz}{dt}\hat{\mathbf{z}}\right) - \zeta_\alpha a\left(\frac{d\alpha}{dt} - \frac{d\phi}{dt}\right)\hat{\mathbf{p}}_2, \quad (3)$$

$$\frac{d\mathbf{M}_c}{dx} + \hat{\mathbf{e}}_3 \times \mathbf{F}_c = \left[\zeta_r\frac{d\phi}{dt} + \zeta_\alpha a^2\left(\frac{d\phi}{dt} - \frac{d\alpha}{dt}\right)\right]\hat{\mathbf{e}}_3, \quad (4)$$

$$\frac{d\mathbf{F}_f}{dx} - \mathbf{K} = \zeta_\alpha a\left(\frac{d\alpha}{dt} - \frac{d\phi}{dt}\right)\hat{\mathbf{p}}_2, \quad (5)$$

$$\frac{d\mathbf{M}_f}{dx} + \hat{\boldsymbol{\varepsilon}}_3 \times \mathbf{F}_f = \zeta_\beta\left(\frac{d\beta}{dt} - \frac{d\alpha}{dt}\right)\hat{\boldsymbol{\varepsilon}}_3, \quad (6)$$

where $\mathbf{F}_c$ and $\mathbf{F}_f$ are the forces on the cell body and flagella, respectively, and $\hat{\mathbf{p}}_2 = \hat{\mathbf{x}} \times \hat{\mathbf{p}}_1$. The normal forces between the flagella and the cell body, $\mathbf{K}$, point in the direction $-\hat{\mathbf{p}}_1$.

To simulate the dynamics of *B. burgdorferi*, we solved Eqs. (3)–(6) using a fourth-order, finite-difference spatial discretization and a semi-implicit time stepping routine. We used a total cell length of 10 μm on a grid of 100 nodes with a time step of 10^{-6} s.

We implement free boundary conditions at both ends of the bacterium, such that there is no total applied force or

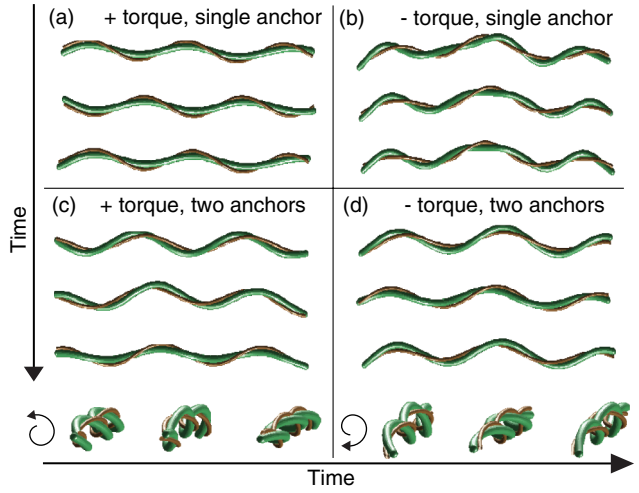

FIG. 2 (color online). Snapshots of the simulated dynamics of *B. burgdorferi*. Simulations were run for a total time of 1–3 s with $a \sim 0.15$ μm, $A_f = 20$ pN μm^2 and $A_c = 10$ pN μm^2. (a),(b) When the flagella are anchored only at a single end of the bacterium, traveling, flat waves are not observed for either positive or negative torques, respectively. (c),(d) When the flagella are anchored at both ends of the bacterium, planar traveling waves result for either positive or negative torques, respectively. Bottom panels show an end-on view of the cases where the flagella are anchored at both ends, which highlights the rotation of the flat-wave shape [21].

moment. Thus, $\mathbf{F}_c + \mathbf{F}_f = 0$ and $\mathbf{M}_c + \mathbf{M}_f = 0$. At $x = 0$ the flagella are anchored into flagellar motors via the flexible hook [16], which redirects the torque from the flagellar motor to be along the tangent vector of the flagellum but is assumed to provide no torque along the direction of $\hat{\mathbf{p}}_1$. Therefore, our boundary conditions at $x = 0$ are $\alpha - \phi = 0$, $\mathbf{M}_f \cdot \hat{\mathbf{p}}_1 = 0$, and $\mathbf{M}_f \cdot \hat{\mathbf{x}} = \tau$. At the other end of the bacterium ($x = L$), we assume torque-free conditions $\mathbf{M}_f \cdot \hat{\mathbf{x}} = 0$. In addition, we either consider that the flagella are long enough to overlap in the center, in which case $\alpha - \phi$ is constant, or zero force on the flagella in the $\hat{\mathbf{p}}_2$ direction, $\mathbf{F}_f \cdot \hat{\mathbf{p}}_2 = 0$.

Using this model, we address the question of whether this physics will produce planar, traveling waves. In the absence of applied torque, we find static flat-wave morphologies, as in Ref. [10]. Starting from this equilibrium shape, we consider the dynamics when the flagellar motors exert torque on the flagella. We begin by considering that the flagella are free at $x = L$, which represents that the flagella from one end do not overlap with flagella from the other end of the bacterium. We further consider that the flagellar motor can rotate in either a clockwise or counter clockwise sense (i.e., the torque from the motor can either be positive or negative) [17]. For both situations we considered a range of cell body and flagellar bending moduli around the biologically measured values (10-80 pN μm^2) [10]. Because the flagella are free at one end, they can readily move and change their circumferential position with respect to the cell body, which drives the cell shape away from a flat wave. For positive torques, we find that the cell body flips into a rotating, helical morphology [Fig. 2(a)]. For negative torques, the cell body converts into a nonplanar undulating and rotating morphology [Fig. 2(b)]. While either of these torques produce cell body undulations or rotation, neither produces planar, traveling waves. For the case where the flagellar ribbon extends from end to end of the bacterium, we find planar, traveling wave solutions for torques in either direction [Figs. 2(c) and 2(d)]. The traveling wave undulates with the rotational speed of the flagella, ω_u. In addition, we also find that the cell body rotates with frequency $\omega_r = \frac{1}{2}(d\beta/dt + d\alpha/dt)$. This rotation is observed experimentally [6] [see also Fig. 1(a)].

The fact that planar, traveling waves require the flagella to be effectively anchored at both ends of the cell suggests that it is important that the length of the flagella in *B. burgdorferi* be long enough to overlap with flagella from the opposite end. As anchoring at both ends seems to be the physiologically relevant scenario, we only consider this case further.

Of the model parameters, the ones that are least known are the flagellar drag coefficients, ζ_α and ζ_β. Therefore, we explored how variations in these parameters affected the dynamics. We found that variations of ζ_α between 10^{-1} and 10^{-3} produced only small decreases in the undulation frequency for positive torque and negative torque and did not noticeably affect cell shape. Variations of ζ_β between

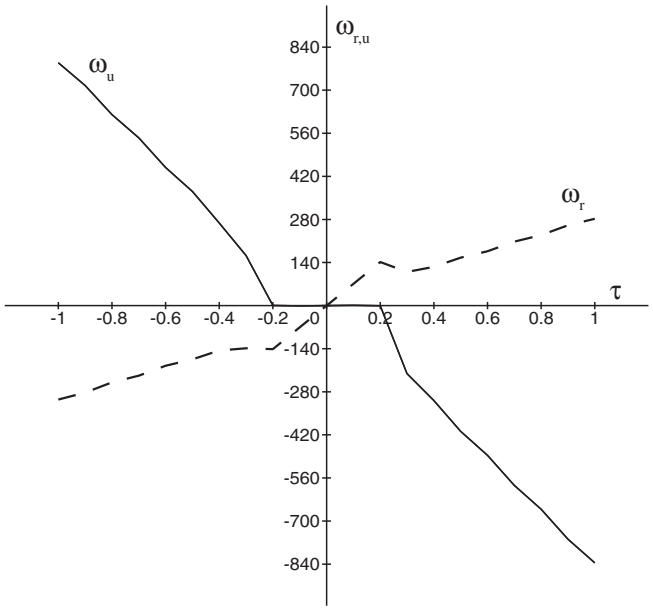

FIG. 3. Flagellar rotational and undulatory frequencies as a function of the torque from the flagellar motor. At low torque, the undulation frequency is near zero, and the cell rotates without undulating. At torques $|\tau| > 0.4$ pN μm, the bacterium swims by undulating and rotating.

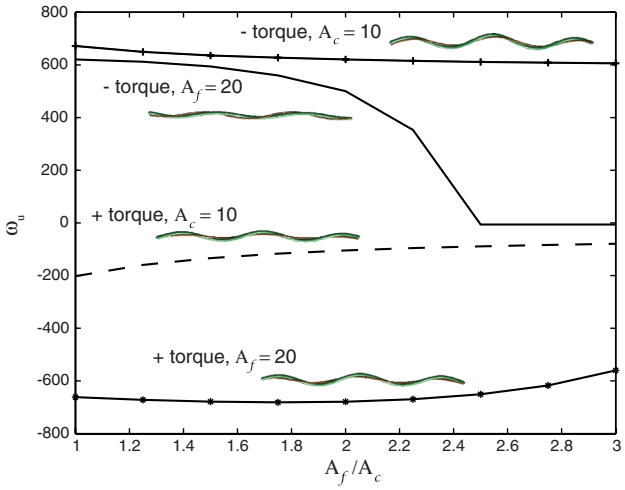

FIG. 4 (color online). The undulation frequency depends on the ratio of A_f/A_c. Increasing this ratio at fixed A_c leads to a decrease in the magnitude of the undulation frequency. When A_f is held fixed, the behavior depends more strongly on the direction of the torque. When the torque is negative and A_c is increased, the cell's undulation frequency drops to zero. The insets show snapshots of the shape of *B. burgdorferi* for the different scenarios.

10^{-4} and 10^{-6} produced a roughly ninefold increase in the bacterium's undulation frequency for positive torque conditions and a roughly fivefold increase under negative torque conditions.

We next looked at how the undulation and rotational frequencies depended on the torque from the flagellar motor. Because the dynamics are highly dissipative, we expected that the undulation frequency would vary linearly with the applied torque. While we found this linear relationship to hold at $|\tau| > 0.4$ pN μm, at low torques the undulation frequency was near zero (Fig. 3). In this low torque regime, the entire cell rotates without undulating. In effect, the applied torque produces crank shafting motions of the flagellum [18]. At larger torques crank shafting (rotation) and speedometer cable motion (undulation) occur [18].

Finally, if the preferred curvature and torsion of the periplasmic flagella are known, then the static shape of *B. burgdorferi* only depends on the ratio of the flagellar bending modulus to the bending modulus of the cell cylinder, A_f/A_c [10]. We, therefore, examined the effect of this ratio on the dynamics of the flat-wave undulation. We began by varying A_f with A_c held fixed at 10 pN μm^2. For positive or negative torques, the magnitude of the undulation frequency decreased with increases in A_f/A_c (Fig. 4). We attribute this decrease in frequency to the fact that as the flagella become more stiff, the amplitude of the flat-wave shape increases [10]. Since the flagellar motor is a roughly constant torque motor [16], balancing the power input from the flagellar motor with the power dissipated by the cell body undulations, we expect that $\omega \propto \tau/\mathcal{A}^2$, which is consistent with our findings. We then varied A_c holding A_f fixed at 20 pN μm^2. For this case, we observed a decrease in the frequency when the flagellar motor torque was negative and the bending moduli ratio was small; however at large values of the ratio, the undulation frequency dropped to zero, thus indicating the presence of crankshaft motion over speedometer cable motion (Fig. 3). For all of these simulations, we found that there was less than a 2%–8% increase in the amplitude between positive and negative torques (Fig. 4 insets). Overall, our simulations provide the best agreement with the experimentally observed morphology and frequency when $A_f/A_c \approx 2$.

In this Letter, we developed a model for the physics of the swimming dynamics of *B. burgdorferi*. This model reproduces the bacterium's planar, traveling wave, but only if the periplasmic flagella are effectively anchored at both ends of the cell, which may explain why the flagella of *B. burgdorferi* are long enough to overlap at the cell middle. Our model predicts that at low torque the cell rotates without undulating, and at higher torque the cell rotates and undulates with distinct frequencies that are roughly linearly proportional to the applied torque. In addition, we predict how these frequencies depend on cell stiffness. Since cell speed is proportional to the undulation frequency [19,20], our results offer testable predictions for how cell speed is affected by mutations or chemical perturbations that affect cell or flagellar stiffness. In addition, this model can serve as a basis for understanding the complex physical interactions between the bacterium and its hosts [5] and should be applicable to the study of other spirochetes, such as *T. pallidum*, the causative agent of syphilis.

This work was supported by the National Institutes of Health Grant No. NIH RO1 GM072004. Useful discussions with Dr. Justin D. Radolf and Michael W. Harman are acknowledged.

[1] N. W. Charon and S. F. Goldstein, Annu. Rev. Genet. **36**, 47 (2002).
[2] N. W. Charon, S. F. Goldstein, M. Marko, C. Hsieh, L. L. Gebhardt, M. A. Motaleb, C. W. Wolgemuth, R. J. Limberger, and N. Rowe, J. Bacteriol. **191**, 600 (2009).
[3] J. D. Radolf, M. J. Caimano, B. Stevenson, and L. T. Hu, Nat. Rev. Microbiol. **10**, 87 (2012).
[4] C. Li, A. Motaleb, M. Sal, S. F. Goldstein, and N. W. Charon, J. Mol. Microbiol. Biotechnol. **2**, 345 (2000).
[5] M. W. Harman, S. M. Dunham-Ems, M. J. Caimano, A. A. Belperron, L. K. Bockenstedt, H. C. Fu, J. D. Radolf, and C. W. Wolgemuth, Proc. Natl. Acad. Sci. U.S.A. **109**, 3059 (2012).
[6] S. F. Goldstein, N. W. Charon, and J. A. Kreiling, Proc. Natl. Acad. Sci. U.S.A. **91**, 3433 (1994).

[7] C. W. Wolgemuth, N. W. Charon, S. F. Goldstein, and R. E. Goldstein, J. Mol. Microbiol. Biotechnol. **11**, 221 (2006).
[8] A. G. Barbour and S. F. Hayes, Microbiol. Rev. **50**, 381 (1986).
[9] B. J. Paster and F. E. Dewhirst, J. Mol. Microbiol. Biotechnol. **2**, 341 (2000).
[10] C. Dombrowski, W. Kan, Md. Abdul Motaleb, N. W. Charon, R. E. Goldstein, and C. W. Wolgemuth, Biophys. J. **96**, 4409 (2009).
[11] W. Kan and C. W. Wolgemuth, Biophys. J. **93**, 54 (2007).
[12] J. Izard *et al.*, J. Bacteriol. **191**, 7566 (2009).
[13] L. D. Landau and E. M. Lifshitz, *Theory of Elasticity* (Pergamon, New York, 1986), 3rd ed..
[14] J. Gray and G. J. Hancock, J. Exp. Biol. **32**, 802 (1955).
[15] J. Yang, G. Huber, and C. W. Wolgemuth, Phys. Rev. Lett. **107**, 268101 (2011).
[16] H. Berg, Annu. Rev. Biochem. **72**, 19 (2003).
[17] We assume that the motor torque is independent of rotational speed; however, in *E. coli*, the motor torque is only constant in the counterclockwise direction but drops linearly with speed in the clockwise direction [J. Yuan, K. A. Fahrner, L. Turner, and H. C. Berg, Proc. Natl. Acad. Sci. U.S.A. **107**, 12 846 (2010)].
[18] R. E. Goldstein, A. Goriely, G. Huber, and C. W. Wolgemuth, Phys. Rev. Lett. **84**, 1631 (2000).
[19] G. I. Taylor, Proc. R. Soc. A **211**, 225 (1952).
[20] A. T. Chwang, H. Winet and T. Y. Wu, Journal of mechanochemistry and cell motility **3**, 69 (1974).
[21] See Supplemental Material http://link.aps.org/supplemental/10.1103/PhysRevLett.109.218104 for movies of the experimental and simulation time courses shown in Figs. 1 and 2.